Biomediation of submarine sediment gravity flow dynamics

Craig, Melissa; Baas, Jaco H.; Amos, Kathryn J. ; Strachan, Lorna J.; Manning, Andrew J.; Paterson, David M.; Hope, Julie A.; Nodder, Scott D.; Baker, Megan L.

Geology

DOI:
10.1130/G46837.1

Published: 01/01/2020

Peer reviewed version

Biomediation of sediment gravity flow dynamics

Melissa J. Craig[1], Jaco H. Baas[2], Kathryn J. Amos[1], Lorna J. Strachan[3], Andrew J. Manning[4], David M. Paterson[5], Julie A. Hope[6], Scott D. Nodder[7], Megan L. Baker[2]

[1]*Australian School of Petroleum, The University of Adelaide, South Australia, Australia*

[2]*School of Ocean Sciences, Bangor University, Menai Bridge, UK*

[3]*School of Environment, University of Auckland, Auckland, NZ*

[4]*HR Wallingford, Howbery Park, Wallingford, UK*

[5]*Scottish Oceans Institute, School of Biology, University of St Andrews, St Andrews, UK*

[6]*Institute of Marine Science, University of Auckland, Auckland, NZ*

[7]*National Institute of Water & Atmospheric Research, Wellington, NZ*

ABSTRACT

Sediment gravity flows are the primary process by which sediment and organic carbon are transported from the continental margin to the deep ocean. Up to 40% of the total marine organic carbon pool is represented by cohesive extracellular polymeric substances (EPS) produced by micro-organisms. The effect of these polymers on sediment gravity flows has not been investigated, despite the economic and societal importance of these flows. We present the first EPS concentrations measured in deep-sea sediment, combined with novel laboratory data that offer insights into the modulation of the dynamics of clay-laden, physically cohesive sediment gravity flows by biological cohesion. We show that EPS can profoundly affect the character, evolution and run-out of sediment gravity flows, and are as prevalent in deep oceans as in shallow seas. Transitional and laminar plug flows are more susceptible to EPS-induced changes in flow properties than turbulent flows. At relatively low concentrations, EPS markedly decrease the head velocity and run-out distance of transitional flows. This biological cohesion is greater, per unit weight, than the physical cohesion of cohesive clay and may exert a stronger control on flow behavior. These results significantly improve our understanding of the effect of an unrealized biological component of sediment gravity flows. The implications are wide ranging and may influence predictive models of sediment gravity flows and advance our understanding how these flows transport and bury organic carbon globally.

INTRODUCTION

Clay, inherently associated with organic matter, is the most abundant sediment type on Earth (Hillier, 1995). Recent advances in our understanding of the properties of clay have redefined our models of submarine sediment gravity flows (SGFs) in both modern and ancient environments (Barker et al., 2008; Sumner et al., 2009; Wright and Friedrichs, 2006). SGFs are volumetrically the most significant sediment transport process in the ocean, pose destructive hazards to offshore infrastructure and their deposits form major hydrocarbon reservoirs (Talling, 2014). Understanding and predicting SGF behaviour therefore has scientific, economic and social importance.

Clay-rich SGFs are governed by the ability of clay minerals to aggregate, or flocculate (McCave and Jones, 1988). Laboratory experiments of clay-rich SGFs show that at sufficiently high concentrations of clay, flocs bind to form a network that behaves as a gel, increasing viscosity and suppressing shear-generated turbulence (Baas and Best, 2002; Baas et al., 2009). These flows, and their deposits, are radically different to fully turbulent flows and highlight the importance of understanding how cohesive material affects SGFs.

Extracellular polymeric substances (EPS) are secreted by microorganisms in many environments, from rivers and estuaries to hypersaline systems and deep-sea hydrothermal vents (Decho and Gutierrez, 2017). The adhesion of this exopolymer to sediment grains forms a matrix of EPS, sediment and single-cell organisms called a biofilm, which is considered the primary mechanism by which benthic microorganisms stabilise the sediment they inhabit (Tolhurst et al., 2002). Small concentrations of EPS (C_{EPS} < 0.063% by weight), representing baseline levels in estuarine sediment, can increase the development time of bedforms exponentially (Malarkey et al., 2015). EPS research to date has focused on coastal environments. The presence of EPS in deep-sea sediment and their impact on SGFs is not known.

EPS represent up to 40% of the marine organic carbon pool (Falkowski et al., 1998). The burial of organic carbon (C_{org}) in marine sediment represents the second largest sink of atmospheric CO_2 (Galy et al., 2007). However, global carbon budget studies typically estimate C_{org} flux by measuring the particulate organic matter settling through the water column and accumulating in marine sediment (Decho and Gutierrez, 2017; Martin et al., 1987; Muller-Karger et al., 2005). SGFs are not currently considered a significant C_{org} transport and burial process in C_{org} flux models on continental margins. This is surprising, since fine-grained sediment flows have been found to transport the majority of C_{org} (de Haas et al., 2002). Here we present the first measurements of EPS from deep-sea sediment cores, and through novel experiments we test if EPS-derived biological cohesion is capable of inhibiting turbulence and intensifying cohesive SGF behaviour. This has fundamental implications for understanding SGF behaviour in the natural environment, models of C_{org} flux on continental margins and estimating C_{org} burial, as well as reconstruction of past environments from ancient deposits and predicting hydrocarbon reservoir properties.

METHODS

To explore the impact of biological cohesion on the dynamics of cohesive SGFs, a series of experimental SGFs were generated, with and without EPS. These flows were generated in a 5 m long, 0.2 m wide, and 0.5 m deep, smooth-bottomed lock-exchange tank (Supplementary Fig. 1). The reservoir was filled with a mixture of kaolinite clay (volumetric concentration C_{vol} = 5-23%), EPS, and seawater. Xanthan gum was used as a proxy for natural EPS (cf. Tan et al., 2014). Xanthan gum shares chemical similarities with a wide variety of EPS and is widely used as a substitute for EPS in marine ecology, soil science and sediment stability research (see Supplementary Methods). The range of EPS dry weight concentrations used in the experiments, C_{EPS} = 0-0.268%, was informed by seabed sediment cores obtained during *RV Tangaroa* cruise TAN1604, from 127 to 1872 m depths in the Hauraki Gulf, NZ (Supplementary Figs 2, 3;

Supplementary Table 1). These EPS data are based on bulk carbohydrate content, collected using the standard assay method of DuBois et al. (1956). The maximum concentration recorded was 0.260% with an average value of 0.139%. For comparison, background EPS content measured in estuarine sediment ranges from 0.01% to 0.1% and from 0.1% to 0.67% in freshwater sediment (Gerbersdorf et al., 2009; Malarkey et al., 2015).

In the laboratory, we compared the head velocity, U_h, and run-out distance of clay-only control flows with equivalent flows containing EPS to test if biological cohesion intensifies cohesive flow behaviour. U_h versus horizontal distance was measured using a high-definition video camera. Flow run-out distances (maximum deposit extent from the lock gate) were recorded, except for flows that travelled the length of the tank (Table 1). To examine the impact of EPS on floc dynamics, samples were extracted for floc size and density analyses, using the LabSFLOC-2 method (Supplementary Methods). Each flow was classified visually following Hermidas et al. (2018).

CONTROL FLOWS WITHOUT EPS

The clay-only control flows generated turbidity currents at C_{vol} = 5-15% and top transitional plug flows (TTPFs; Hermidas et al. (2018)) at C_{vol} = 22-23%, allowing us to examine the effect of EPS in fully turbulent flows and transitional flows experiencing turbulence suppression by physical cohesion (Table 1). Turbidity currents travelled the length of the tank and generated shear waves along their upper interface with the ambient fluid (Table 2). The TTPFs featured a dense, laminar lower 'plug' layer with coherent fluid entrainment structures (Baker et al., 2017; Supplementary Figs 4, 5) that transitioned upwards into a dilute turbulent layer (Table 2).

FLOWS WITH EPS

Adding EPS to the turbidity currents with C_{vol} < 15% produced no visual changes in flow behaviour and no measurable differences in the U_h profiles (Supplementary Figs 6, 7). At C_{vol} = 15%, the EPS-laden flows (Table 1) were also visually indistinguishable from turbulent clay-only F07. However, U_h of F08 and F09 decreased more rapidly than for F07 between 4-4.2 m along the tank, resulting in lower U_h values at 4.6 m (Fig. 1). Highest C_{EPS} F10 began to decelerate rapidly at 2.5 m, and halted at 3.9 m.

The 22% and 23% clay TTPFs exhibited distinct decreases in U_h and run-out distance as EPS were added (Fig. 2, Supplementary Fig. 8). Normalized to the maximum head velocity, $U_{h,max}$, and run-out distance of the clay-only flows, the combined 22% and 23% data are strongly correlated with C_{EPS} (Supplementary Figs 9, 10). In 22% clay flows, $C_{EPS} \leq 0.089\%$ still produced TTPFs with lower $U_{h,max}$ and shorter run-out distance than the control (Supplementary Fig. 8), whereas $C_{EPS} \geq 0.133\%$ dramatically reduced upper boundary mixing, producing a distinct interface with the ambient fluid characteristic of plug flows (Supplementary Fig. 11; Hermidas et al., 2018). F14 and F15 also lacked coherent fluid entrainment structures. These flows achieved $U_{h,max}$ less than half of the 22% clay-only and the clay─EPS TTPFs, and *en-masse* freezing significantly reduced run-out distance (Supplementary Fig. 8). At C_{vol} = 23%, this change from TTPF to plug flow occurred at $C_{EPS} \geq 0.087\%$. At the highest C_{EPS} of 0.259% in F20, the slurry slid out of the reservoir for 0.6 m (Hampton et al., 1996).

ANALYZING THE EFFECT OF EPS ON FLOW PROPERTIES

Our experiments demonstrate that the strong biological cohesion imparted by EPS in the seabed extends to SGFs at C_{EPS} found in deep-sea and coastal environments. U_h and run-out distance were reduced by adding EPS to the TTPFs and the densest turbidity currents. At higher clay and EPS concentrations, the biological cohesion caused flow transformation, suggesting that

EPS limit shear turbulence by increasing the strength of the bonds between clay flocs. These flows are likely to be non-Newtonian with a yield stress, as in aqueous xanthan gum solutions and xanthan-kaolinite mixtures (Hamed and Belhadri, 2009; Song et al., 2006). This biological cohesion was greater per unit weight than the physical cohesion. At 22% clay, the addition of 0.133% EPS induced a flow transformation from TTPF to plug flow, substantially reducing the run-out distance and $U_{h,max}$. A similar reduction in run-out distance would require an increase in clay concentration from 22% to 25% in an EPS-free flow (Baker et al., 2017).

We hypothesise that EPS strengthen cohesion between flocs and assists in building a network of interconnected flocs (Leppard and Droppo, 2004). EPS in TTPFs are brought into contact with more clay particles than in turbidity currents, allowing the EPS to strengthen the particle network, further suppress turbulence and encourage laminar flow (Table 2).

To test this hypothesis, samples of fluid were taken from clay-only TTPF F16 and clay─EPS TTPF F17 for floc size and density comparison using LabSFLOC-2 (Supplementary Fig. 12). As each sample was released into the settling column, the gel underwent gravitational settling and broke into flocs. Only 10% of the flocs in F16 were larger than 200 μm, compared to 55% in F17. The clay─EPS flocs had a lower density than the clay-only flocs and this difference increased up to ten times as floc size increased. The dominance of large, water-rich flocs in the clay─EPS F17 implies that the clay─EPS gel was more resistant to breaking into smaller flocs under shear during static settling. We further infer that within flows, these water-rich clay─EPS flocs are more resistant to shear turbulence than the clay-only flocs, and that this difference increases with increasing clay and EPS concentration, resulting in more laminar flow behaviour.

EPS IN NATURAL SEDIMENT GRAVITY FLOWS

150 The influence of EPS was observed in experimental turbulent, transitional, and laminar SGFs,
151 each with complex and variable flow properties. Scaling of these flows to natural prototypes is
152 a non-trivial task, and standard methods (e.g. Froude, Reynolds, Shields, and distorted
153 geometric scaling) are unlikely to be valid without modification (Iverson, 1997; Marr et al.,
154 2001; Mulder and Alexander, 2001). However, the experimental SGFs may be used as
155 analogue for natural SGFs based on fundamental physical principles. The experimental flows
156 travelled at <0.55 ms^{-1}; suitable analogues are hyperpycnal river discharge, and weak
157 submarine SGFs triggered by earthquakes with velocities of 0.3-1.6 ms^{-1} (Talling et al., 2013),
158 and natural SGFs that have decelerated to a similar velocity. The observed turbulence
159 suppression is likely to apply to other flow types, such as wave and current-driven sediment
160 flows and fluid mud flows on shelves, which rely on turbulence to suspend particles
161 (Traykovski et al., 2000). Turbulence modulation in higher velocity flows, and in flows with
162 higher turbulence intensity, is likely to occur at higher concentrations of EPS and clay than in
163 these experiments.

164 **IMPLICATIONS FOR THE GLOBAL CARBON CYCLE**

165 The settling of particulate C_{org} to the seafloor is regarded as a key process in the global carbon
166 cycle. However, measurements show that only 1-4% of this material is buried within the seabed
167 (Decho and Gutierrez, 2017). Large amounts of particulate C_{org} are delivered to continental
168 shelves via rivers (0.8 PgC y^{-1}; Liu et al., 2010) and *in situ* primary production (6.2 PgC y^{-1};
169 Chen, 2010). The majority is remineralized in the water column and only a small amount
170 preserved on the shelf (0.2 PgC y^{-1}; Chen, 2010; de Haas et al., 2002; Liu et al., 2010). In
171 contrast, continental slopes are an important carbon sink. Around 40-50% of C_{org} transported
172 from the shelf to the continental slope (0.5 PgC y^{-1}; Chen, 2010) is buried at water depths <500
173 m. The remaining 50-60% is stored at >800 m (Muller-Karger et al., 2005).

The transport of C_{org} down continental slopes by SGFs has not received much attention in these calculations. However, large-scale SGFs on continental margins have the potential to move large quantities of terrestrial and marine C_{org} to the deep-sea (e.g., Mountjoy et al., 2018) whilst also providing the rapid burial that promotes the preservation of $C_{org.}$ The ability of EPS to alter SGF behaviour, shown here, implies that EPS change the spatial distribution of organic carbon sinks. Moreover, the increased cohesion of mixed clay-EPS flows promotes *en masse* deposition which helps the burial and preservation of C_{org} by reducing oxygen exposure times (Burdige, 2007; Hedges and Keil, 1995). In the context of the global carbon cycle, a better understanding of the ability of EPS to influence the dynamics of its transport medium may improve numerical models of C_{org} fluxes on continental margins particularly where they are dominated by fine-grained sediment input and high primary, and therefore EPS, production. Our deep-sea cores show EPS levels similar to coastal environments, where EPS are widely recognised for its contribution to the C_{org} pool (Morelle et al., 2017). These results highlight that current global carbon budgets may underestimate C_{org} flux by not considering C_{org} transport via SGFs and the contribution of in-situ EPS to the C_{org} sink in deep-sea sediment.

CONCLUDING REMARKS

An increasing number of studies highlight the importance of considering physical cohesion when interpreting and modelling SGF processes, but the insights into biologically cohesive SGFs presented here indicate the need to recognise the potent effects of EPS in future studies. At the concentrations found in modern estuarine, coastal and deep marine environments, EPS have proven to be capable of changing flow behaviour and reducing the deposit run-out distance and $U_{h,max}$ of cohesive flows. This research improves our predictive models of these volumetrically significant and hazardous events. Further studies are needed to better constrain and quantify the effects of EPS in process models for cohesive and non-cohesive SGFs, and their wider environmental relevance for geological history and the global carbon cycle.

ACKNOWLEDGEMENTS

The Australian Government Research Training Program Scholarship funded M.J.C.'s PhD candidature. An International Association of Sedimentologists Postgraduate Award Grant funded M.J.C.'s visit to Bangor University. The U.K. Natural Environment Research Council grant NE/1027223/1 (COHBED project) enabled this research to be undertaken using the flume facility built by Rob Evans (Bangor University). We thank Brian Scannell, Edward Lockhart and Connor McCarron for help in the laboratory. We thank the officers, crew and scientific complement for core collection and processing on TAN1604, with funding via the New Zealand Strategic Science Investment Fund to NIWA's National Centres of 'Coasts & Oceans' and 'Climate, Atmosphere & Hazards'. Irvine Davidson (University of St Andrews) is thanked for his help in measuring EPS concentrations in the Hauraki Gulf cores.

REFERENCES CITED

Baas, J. H., and Best, J. L., 2002, Turbulence modulation in clay-rich sediment-laden flows and some implications for sediment deposition: Journal of Sedimentary Research, v. 72, no. 3, p. 336-340.

Baas, J. H., Best, J. L., Peakall, J., and Wang, M., 2009, A phase diagram for turbulent, transitional, and laminar clay suspension flows: Journal of Sedimentary Research, v. 79, no. 4, p. 162-183.

Baker, M. L., Baas, J. H., Malarkey, J., Jacinto, R. S., Craig, M. J., Kane, I. A., and Barker, S., 2017, The Effect of Clay Type On the Properties of Cohesive Sediment Gravity Flows and Their Deposits: Journal of Sedimentary Research, v. 87, no. 11, p. 1176-1195.

Barker, S. P., Haughton, P. D., McCaffrey, W. D., Archer, S. G., and Hakes, B., 2008, Development of rheological heterogeneity in clay-rich high-density turbidity currents: Aptian Britannia Sandstone Member, UK continental shelf: Journal of Sedimentary Research, v. 78, no. 2, p. 45-68.

Burdige, D. J., 2007, Preservation of organic matter in marine sediments: controls, mechanisms, and an imbalance in sediment organic carbon budgets?: Chemical reviews, v. 107, no. 2, p. 467-485.

Chen, C.-T. A., 2010, Cross-boundary exchanges of carbon and nitrogen in continental margins, Carbon and Nutrient Fluxes in Continental Margins, Springer, p. 561-574.

de Haas, H., van Weering, T. C., and de Stigter, H., 2002, Organic carbon in shelf seas: sinks or sources, processes and products: Continental Shelf Research, v. 22, no. 5, p. 691-717.

Decho, A. W., and Gutierrez, T., 2017, Microbial extracellular polymeric substances (EPSs) in ocean systems: Frontiers in microbiology, v. 8, p. 922.

DuBois, M., Gilles, K. A., Hamilton, J. K., Rebers, P. t., and Smith, F., 1956, Colorimetric method for determination of sugars and related substances: Analytical chemistry, v. 28, no. 3, p. 350-356.

Falkowski, P. G., Barber, R. T., and Smetacek, V., 1998, Biogeochemical controls and feedbacks on ocean primary production: Science, v. 281, no. 5374, p. 200-206.

Galy, V., France-Lanord, C., Beyssac, O., Faure, P., Kudrass, H., and Palhol, F., 2007, Efficient organic carbon burial in the Bengal fan sustained by the Himalayan erosional system: Nature, v. 450, no. 7168, p. 407.

Gerbersdorf, S. U., Westrich, B., and Paterson, D. M., 2009, Microbial extracellular polymeric substances (EPS) in fresh water sediments: Microbial ecology, v. 58, no. 2, p. 334-349.

Hamed, S. B., and Belhadri, M., 2009, Rheological properties of biopolymers drilling fluids: Journal of Petroleum Science and Engineering, v. 67, no. 3-4, p. 84-90.

Hampton, M. A., Lee, H. J., and Locat, J., 1996, Submarine landslides: Reviews of geophysics, v. 34, no. 1, p. 33-59.

Hedges, J. I., and Keil, R. G., 1995, Sedimentary organic matter preservation: an assessment and speculative synthesis: Marine chemistry, v. 49, no. 2-3, p. 81-115.

Hermidas, N., Eggenhuisen, J. T., Jacinto, R. S., Luthi, S. M., Toth, F., and Pohl, F., 2018, A Classification of Clay-Rich Subaqueous Density Flow Structures: Journal of Geophysical Research: Earth Surface, v. 123, no. 5, p. 945-966.

Hillier, S., 1995, Erosion, sedimentation and sedimentary origin of clays, Origin and Mineralogy of Clays, Springer, p. 162-219.

Iverson, R. M., 1997, The Physics of Debris Flows: Reviews of Geophysics, v. 35, no. 3, p. 245-296.

Leppard, G. G., and Droppo, I. G., 2004, Overview of flocculation processes in freshwater ecosystems, Flocculation in Natural and Engineered Environmental Systems, CRC Press, p. 25-46.

Liu, K.-K., Atkinson, L., Quiñones, R. A., and Talaue-McManus, L., 2010, Biogeochemistry of continental margins in a global context, Carbon and Nutrient Fluxes in Continental Margins, Springer, p. 3-24.

Malarkey, J., Baas, J. H., Hope, J. A., Aspden, R. J., Parsons, D. R., Peakall, J., Paterson, D. M., Schindler, R. J., Ye, L., Lichtman, I. D., Bass, S. J., Davies, A. G., Manning, A. J., and Thorne, P. D., 2015, The pervasive role of biological cohesion in bedform development: Nature Communications, v. 6, p. 6257.

Marr, J. G., Harff, P. A., Shanmugam, G., and Parker, G., 2001, Experiments on subaqueous sandy gravity flows: the role of clay and water content in flow dynamics and depositional structures: Geological Society of America Bulletin, v. 113, no. 11, p. 1377-1386.

Martin, J. H., Knauer, G. A., Karl, D. M., and Broenkow, W. W., 1987, VERTEX: carbon cycling in the northeast Pacific: Deep Sea Research Part A. Oceanographic Research Papers, v. 34, no. 2, p. 267-285.

277 McCave, I., and Jones, K., 1988, Deposition of ungraded muds from high-density non-
278 turbulent turbidity currents: Nature, v. 333, no. 6170, p. 250-252.
279 Morelle, J., Schapira, M., and Claquin, P., 2017, Dynamics of phytoplankton productivity and
280 exopolysaccharides (EPS and TEP) pools in the Seine Estuary (France, Normandy)
281 over tidal cycles and over two contrasting seasons: Marine environmental research, v.
282 131, p. 162-176.
283 Mountjoy, J. J., Howarth, J. D., Orpin, A. R., Barnes, P. M., Bowden, D. A., Rowden, A. A.,
284 Schimel, A. C., Holden, C., Horgan, H. J., and Nodder, S. D., 2018, Earthquakes drive
285 large-scale submarine canyon development and sediment supply to deep-ocean
286 basins: Science advances, v. 4, no. 3, p. eaar3748.
287 Mulder, T., and Alexander, J., 2001, The physical character of subaqueous sedimentary
288 density flows and their deposits: Sedimentology, v. 48, no. 2, p. 269-299.
289 Muller-Karger, F. E., Varela, R., Thunell, R., Luerssen, R., Hu, C., and Walsh, J. J., 2005,
290 The importance of continental margins in the global carbon cycle: Geophysical
291 Research Letters, v. 32, no. 1.
292 Song, K.-W., Kim, Y.-S., and Chang, G.-S., 2006, Rheology of concentrated xanthan gum
293 solutions: Steady shear flow behavior: Fibers and Polymers, v. 7, no. 2, p. 129-138.
294 Sumner, E. J., Talling, P. J., and Amy, L. A., 2009, Deposits of flows transitional between
295 turbidity current and debris flow: Geology, v. 37, no. 11, p. 991-994.
296 Talling, P. J., 2014, On the triggers, resulting flow types and frequencies of subaqueous
297 sediment density flows in different settings: Marine Geology, v. 352, p. 155-182.
298 Talling, P. J., Paull, C. K., and Piper, D. J., 2013, How are subaqueous sediment density
299 flows triggered, what is their internal structure and how does it evolve? Direct
300 observations from monitoring of active flows: Earth-Science Reviews, v. 125, p. 244-
301 287.
302 Tan, X., Hu, L., Reed, A. H., Furukawa, Y., and Zhang, G., 2014, Flocculation and particle
303 size analysis of expansive clay sediments affected by biological, chemical, and
304 hydrodynamic factors: Ocean Dynamics, v. 64, no. 1, p. 143-157.
305 Tolhurst, T., Gust, G., and Paterson, D., 2002, The influence of an extracellular polymeric
306 substance (EPS) on cohesive sediment stability: Proceedings in Marine Science, v. 5,
307 p. 409-425.
308 Traykovski, P., Geyer, W. R., Irish, J., and Lynch, J., 2000, The role of wave-induced
309 density-driven fluid mud flows for cross-shelf transport on the Eel River continental
310 shelf: Continental Shelf Research, v. 20, no. 16, p. 2113-2140.

311 Wright, L., and Friedrichs, C., 2006, Gravity-driven sediment transport on continental
312 shelves: a status report: Continental Shelf Research, v. 26, no. 17-18, p. 2092-2107.

313

314

315 ***Table 1*** *Basic experimental data. Flow classifications follow the scheme of Hermidas et al.*
316 *(2018). ROD = run-out distance; $U_{h,max}$ = maximum head velocity; TTPF = top transitional*
317 *plug flow.*

Flow	Kaolinite C_{vol} (%)	EPS weight (%)	ROD (m)	$U_{h,max}$ (m s^{-1})	Flow Classification
F01	5	0	-	0.377	Turbidity Current
F02	5	0.134	-	0.379	Turbidity Current
F03	5	0.250	-	0.381	Turbidity Current
F04	10	0	-	0.367	Turbidity Current
F05	10	0.132	-	0.353	Turbidity Current
F06	10	0.264	-	0.348	Turbidity Current
F07	15	0	-	0.430	Turbidity Current
F08	15	0.066	-	0.417	Turbidity Current
F09	15	0.133	-	0.416	Turbidity Current
F10	15	0.265	3.91	0.420	Turbidity Current
F11	22	0	4.69	0.552	TTPF
F12	22	0.067	3.63	0.455	TTPF
F13	22	0.089	3.20	0.438	TTPF
F14	22	0.133	2.13	0.217	Plug Flow
F15	22	0.265	0.92	0.194	Plug Flow
F16	23	0	3.66	0.471	TTPF
F17	23	0.052	2.94	0.439	TTPF
F18	23	0.087	1.80	0.419	Plug Flow
F19	23	0.130	1.32	0.211	Plug Flow
F20	23	0.259	0.60	0.160	Slide

318

319 ***Table 2*** *Summary of flow classifications following the scheme of Hermidas et al. (2018), and concept*
320 *diagrams of flow behaviour and floc characteristics.*

Flow Classification	Experimental Flows	Flow Diagram *(not to scale)*
Turbidity Current	F01–F10	
Top Transitional Plug Flow (TTPF)	F11-F13, F16, F17	
Plug Flow	F14, F15, F18, F19	
Slump	F20	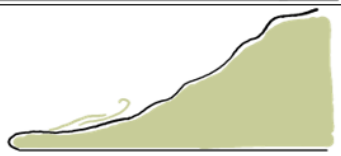

Floc Concept Diagram – Turbidity Current	Floc Concept Diagram – Plug Flow with EPS
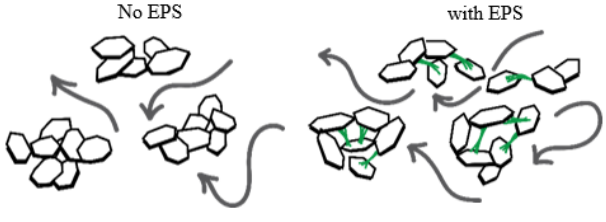	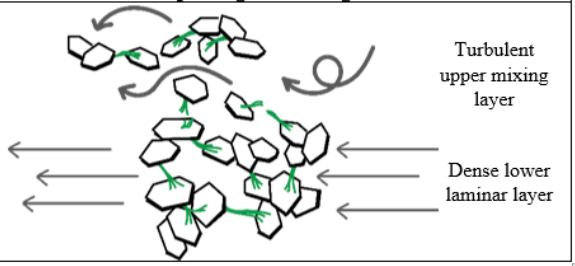

321

322

Figure 1 *Head velocity of 15% kaolinite flows against distance travelled along the tank. Number above the abscissa indicate run-out distances of flow. Values in legend correspond to EPS concentration added to the flow.*

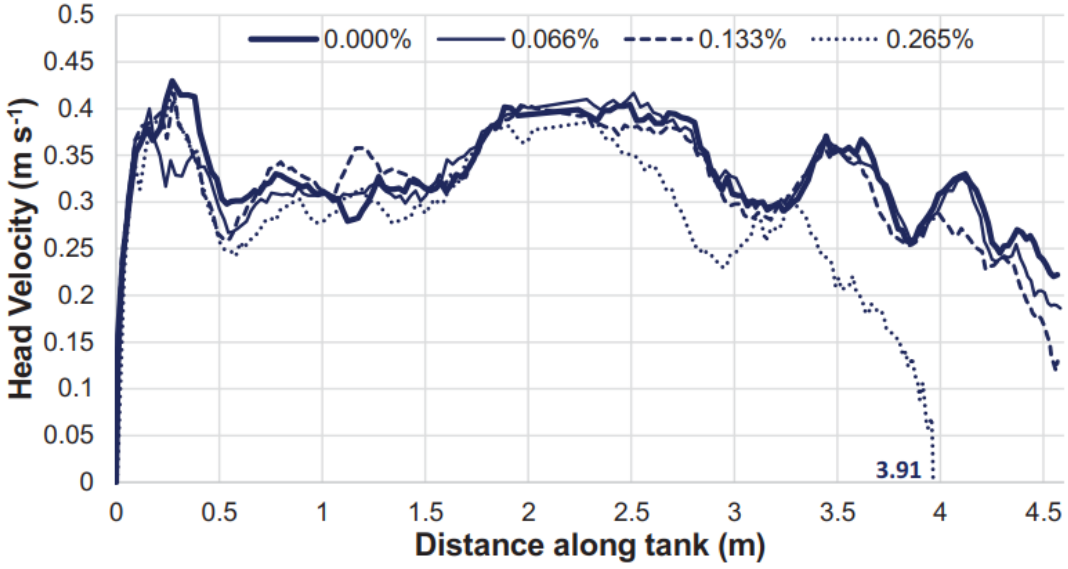

323

Figure 2 *Head velocity of 23% kaolinite flows against distance travelled along the tank. Number above abscissa indicate run-out distances of flow. Values in legend correspond to EPS concentration added to the flow.*

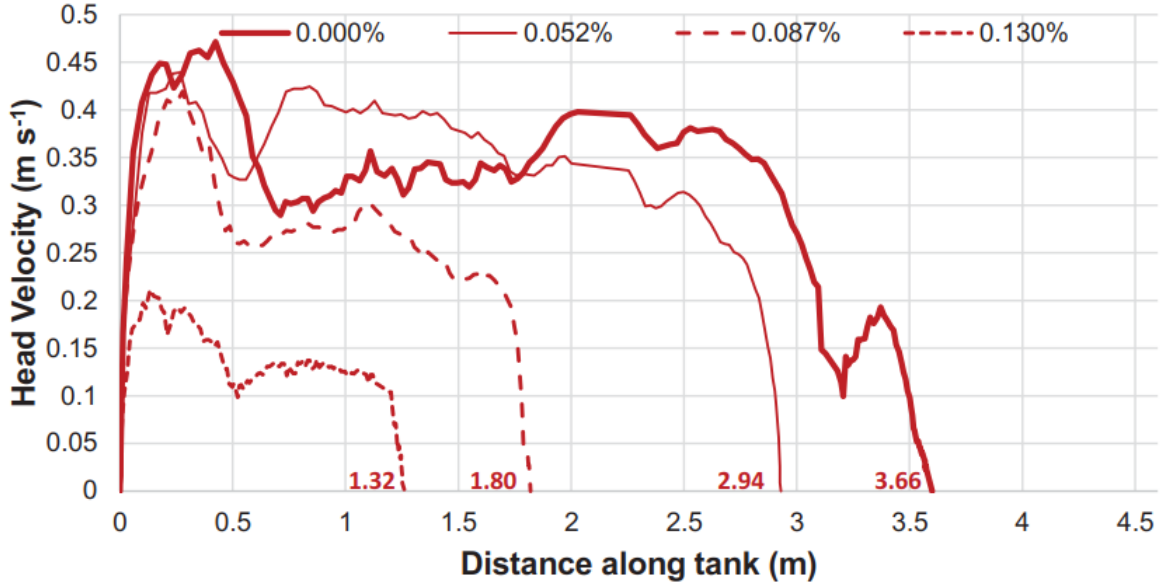

SUPPLEMENTARY INFORMATION

Methodology

Use of Xanthan Gum as an analogue for EPS

Xanthan gum, produced by the bacterium *Xanthomonas campestris*, was used as an analogue for EPS in these experiments because of its chemical and physical similarities with naturally occurring EPS (Steele et al., 2014). It has been common practice in a wide range of studies to substitute EPS for xanthan gum to simplify experiments and control conditions otherwise not possible when working with live bacteria (Rosenzweig et al., 2012).

Xanthan gum is not representative of all naturally occurring EPS. The diverse number of microorganisms that produce EPS, e.g. microalgae, phytoplankton, sea-ice diatoms, estuarine diatoms, bacteria and zooplankton, all secrete EPS with differ compositions for different functions i.e. adhesion, water retention, nutrient source, and enzyme activity (Krembs et al., 2011; Xiao and Zheng, 2016). The use of xanthan as a substitute for EPS in flume experiments is supported by the comparable rheological properties of aqueous solutions of natural EPS and xanthan because of their similarly high molecular weight (Fonseca et al., 2011; Morris et al., 2001; Xiao and Zheng, 2016). Some micro-algae produce polysaccharides that act as better drag-reducing additives than xanthan, rendering xanthan a possibly conservative choice of polymer to demonstrate the potential effects of EPS on sediment gravity flow dynamics (Gasljevic et al., 2008). Xanthan gum also enhances flocculation with increasing salinity in the same way as natural marine biopolymers; it is therefore suitable for use in a sediment-seawater mixtures representative of the marine environment (Furukawa et al., 2014). Beyond this, xanthan gum has been applied as an EPS analogue in studies of the protection of cells from hypersaline shock by EPS (Steele et al., 2014), EPS alteration of the formation of microstructures and salt retention in sea-ice (Krembs et al., 2011), and the effect of EPS on water retention in biofilm-affected soils (Rosenzweig et al., 2012).

Flume Experiments

In order to determine the effect of biological cohesion on physically-cohesive sediment gravity flows, 20 laboratory experiments were conducted in a 5.0 m long, 0.2 m wide and 0.5 m deep smooth-bottomed lock-exchange tank (Supplementary Figure 1). A 0.31 m long reservoir at the upstream end of the tank was filled with a mixture of kaolinite clay (D_{50} = 9.1 μm), EPS, and seawater to a depth of 0.35 m. The remainder of the tank contained seawater to the same

depth. All seawater was sourced from the Menai Strait (North Wales, United Kingdom). Xanthan gum, a commercially available anionic hydrophilic biopolymer, was used as a proxy for natural EPS. The two compartments of the tank were separated by a lock gate, which was lifted to generate the gravity flow.

To account for any time-dependent behaviour of the mixture, each suspension was prepared using the same method. First, the xanthan gum and kaolinite clay were mixed dry in a concrete mixer for 10 minutes to evenly disperse the EPS within the clay. The seawater was then added to and mixed with the dry material for 10 min in the concrete mixer. Next, the wet mixture was decanted into a container and mixed again for 3 min using a handheld concrete mixer to break up any remaining clumps of sediment, before leaving it to rest for 60 min. At the end of the resting time, the suspension was mixed a third time for 3 min and then added to the reservoir of the lock-exchange tank. Here, it was mixed for a final 30 seconds; immediately thereafter the lock gate was lifted as quickly as possible to generate the sediment gravity flow.

A high-definition video camera tracked the head of the flow as it progressed along the tank. The velocity of the head of the flow was calculated using the time-stamped video frames and a reference scale along the bottom of the tank.

LabSFLOC-2 Methodology

Floc properties were measured using the LabSFLOC-2 (Laboratory Spectral Flocculation Characteristics) method. This method has been used successfully in numerous laboratory- and field-based flocculation studies and has demonstrated minimal floc disruption during acquisition (Manning et al., 2007; Mietta et al., 2009). LabSFLOC-2 uses a non-intrusive Puffin Paescon UTC 341 high-resolution video camera positioned 75 mm above the base of a square settling column (190x10x10 mm). This camera observes particles settling in the centre of the column, using a depth of view of 1 mm at 45 mm in front of the lens. For the present experiments, the settling column was filled with seawater from the Menai Strait. To minimize density contrasts, care was taken to match the temperature with that of the seawater in the lock-exchange tank. A 0.4 m long glass pipette (4 mm internal diameter) was positioned in the lock-exchange tank at 60% of the anticipated flow run-out distance (based on an average of 12 replicate experiments). The end of the pipette was placed at 12 mm above the base of the tank, at the approximate height of the velocity maximum, informed by ultrasonic Doppler velocity profiler (UDVP) data. A small volume of mixed water, clay and EPS was then extracted from

388 the passing head of the flow and immediately transferred to the LabSFLOC-2 settling column
389 to minimise particle settling within the pipette. The sample was released from the pipette with
390 the aperture of the pipette in contact with the water surface in the settling column through
391 gravitational settling.

392

393 **REFERENCES CITED**

394 Fonseca, P. R., Dekker, R. F., Barbosa, A. M., Silveira, J. L., Vasconcelos, A. F., Monteiro,
395 N. K., Aranda-Selverio, G., and Da Silva, M. d. L. C., 2011, Thermal and rheological
396 properties of a family of botryosphaerans produced by Botryosphaeria rhodina
397 MAMB-05: Molecules, v. 16, no. 9, p. 7488-7501.
398 Furukawa, Y., Reed, A. H., and Zhang, G., 2014, Effect of organic matter on estuarine
399 flocculation: a laboratory study using montmorillonite, humic acid, xanthan gum, guar
400 gum and natural estuarine flocs: Geochemical transactions, v. 15, no. 1, p. 1.
401 Gasljevic, K., Hall, K., Chapman, D., and Matthys, E., 2008, Drag-reducing polysaccharides
402 from marine microalgae: species productivity and drag reduction effectiveness:
403 Journal of applied phycology, v. 20, no. 3, p. 299-310.
404 Krembs, C., Eicken, H., and Deming, J. W., 2011, Exopolymer alteration of physical
405 properties of sea ice and implications for ice habitability and biogeochemistry in a
406 warmer Arctic: Proceedings of the National Academy of Sciences, v. 108, no. 9, p.
407 3653-3658.
408 Manning, A., Friend, P., Prowse, N., and Amos, C., 2007, Estuarine mud flocculation
409 properties determined using an annular mini-flume and the LabSFLOC system:
410 Continental Shelf Research, v. 27, no. 8, p. 1080-1095.
411 Mietta, F., Chassagne, C., Manning, A. J., and Winterwerp, J. C., 2009, Influence of shear
412 rate, organic matter content, pH and salinity on mud flocculation: Ocean Dynamics, v.
413 59, no. 5, p. 751-763.
414 Morris, G., Li, P., Puaud, M., Liu, Z., Mitchell, J., and Harding, S., 2001, Hydrodynamic
415 characterisation of the exopolysaccharide from the halophilic cyanobacterium
416 Aphanothece halophytica GR02: A comparison with xanthan: Carbohydrate
417 Polymers, v. 44, no. 3, p. 261-268.
418 Rosenzweig, R., Shavit, U., and Furman, A., 2012, Water retention curves of biofilm-affected
419 soils using xanthan as an analogue: Soil Science Society of America Journal, v. 76,
420 no. 1, p. 61-69.

Steele, D. J., Franklin, D. J., and Underwood, G. J., 2014, Protection of cells from salinity stress by extracellular polymeric substances in diatom biofilms: Biofouling, v. 30, no. 8, p. 987-998.

Xiao, R., and Zheng, Y., 2016, Overview of microalgal extracellular polymeric substances (EPS) and their applications: Biotechnology advances, v. 34, no. 7, p. 1225-1244.

Supplementary Table 1 Summary of EPS data from cores collected during RV Tangaroa cruise TAN1604 in the outer Hauraki Gulf, New Zealand.

Core	*Depth (mm)*	*Total Carbohydrate, mean (%)*	*Total Carbohydrate, standard deviation (%)*	*D_{50} (µm)*	*Textural Description*
CS07	0-10	0.0833	0.0173	125.6	Slightly Gravelly Muddy Sand
CS07	10-20	0.0850	0.0099	97.42	Muddy Sand
CS07	20-30	0.0834	0.0109	69.52	Muddy Sand
CS07	30-40	0.1798	0.0680	49.23	Sandy Mud
CS10	0-10	0.1685	0.0395	74.75	Muddy Sand
CS10	10-20	0.1789	0.0145	88.49	Muddy Sand
CS10	20-30	0.1864	0.0143	93.73	Muddy Sand
CS10	30-40	0.1809	0.0201	93.73	Muddy Sand
CS10	40-50	0.1644	0.0192	93.73	Muddy Sand
CS10	50-60	0.1724	0.0136	81.16	Muddy Sand
CS10	60-70	0.1696	0.0192	81.61	Muddy Sand
CS10	70-80	0.1655	0.0232	82.68	Muddy Sand
CS10	80-90	0.1592	0.0313	77.13	Muddy Sand
CS14	0-10	0.0918	0.0237	64.69	Muddy Sand
CS14	10-20	0.0864	0.0150	63.01	Muddy Sand
CS14	20-30	0.1041	0.0153	81.13	Muddy Sand
CS14	30-40	0.1222	0.0065	81.13	Muddy Sand
CS14	40-50	0.0825	0.0173	81.13	Muddy Sand
CS14	50-55	0.0887	0.0117	83.05	Muddy Sand
CS14	55-60	0.0941	0.0109	83.05	Muddy Sand
CS14	60-65	0.0947	0.0193	71.57	Muddy Sand
CS19	0-10	0.1801	0.0368	15.00	Mud
CS19	10-20	0.1960	0.0477	15.44	Sandy Mud
CS19	20-30	0.2104	0.0180	14.88	Mud
CS19	30-40	0.2597	0.0753	14.42	Mud
CS19	40-50	0.2158	0.0777	14.33	Mud
CS19	50-60	0.1010	0.0172	15.53	Sandy Mud
CS19	60-70	0.1350	0.0779	20.16	Sandy Mud
CS19	70-80	0.0879	0.0248	18.47	Sandy Mud
CS19	80-90	0.1041	0.0477	17.16	Sandy Mud
CS19	90-100	0.0867	0.0290	16.28	Sandy Mud

SUPPLEMENTARY FIGURES

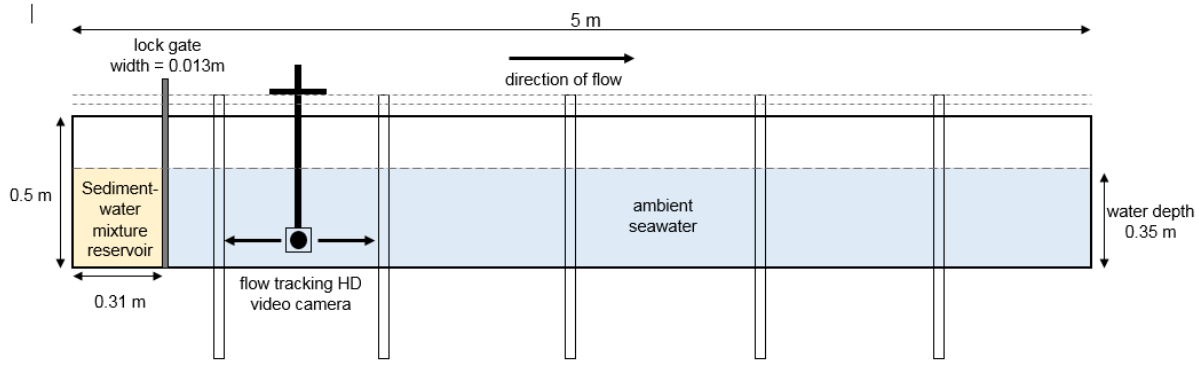

Supplementary Figure 1 Schematic drawing of the lock-exchange tank.

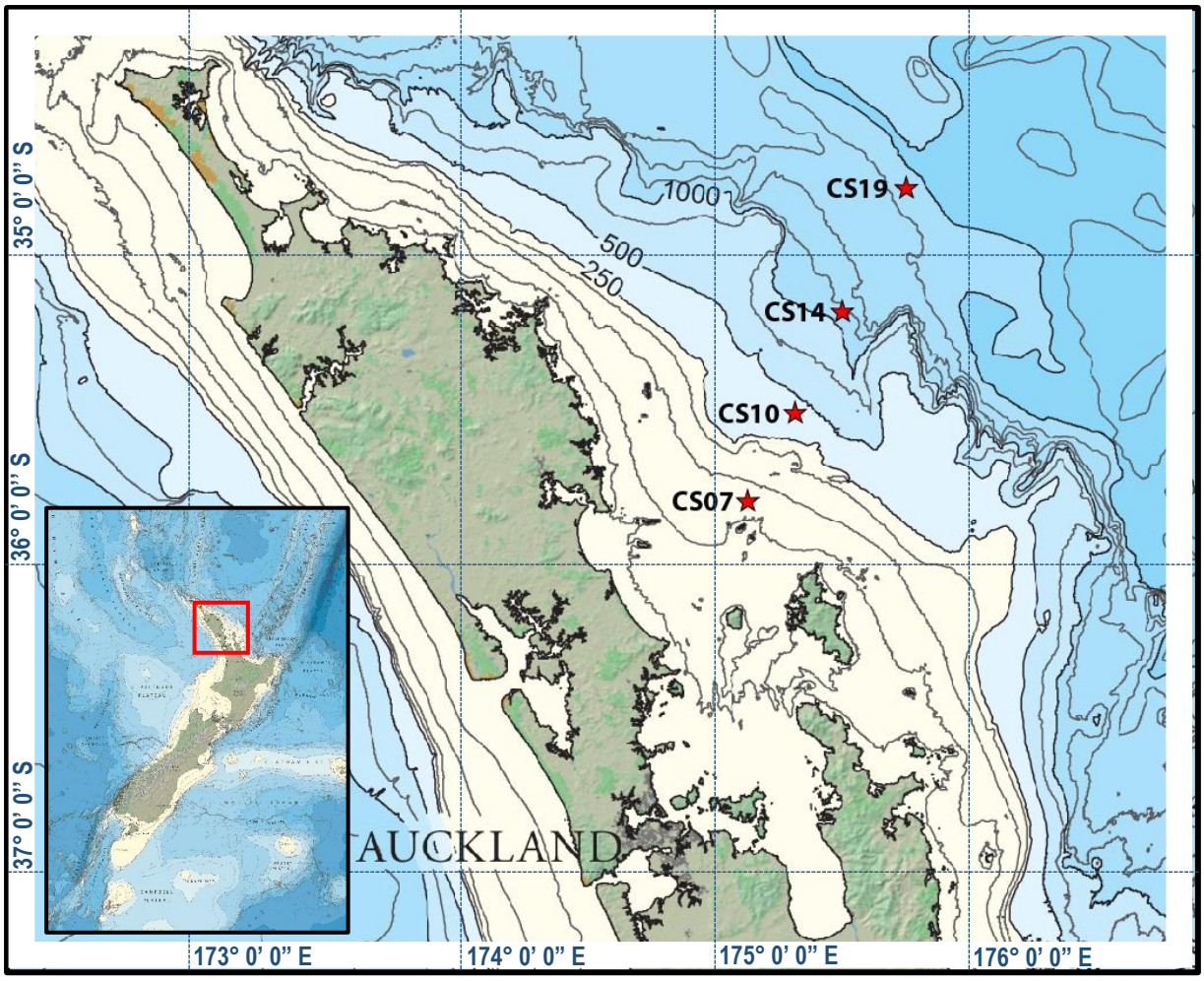

Supplementary Figure 2 Outer Hauraki Gulf, New Zealand (see inset) with locations of core samples CS07 (127 m water depth), CS10 (432 m), CS14 (1149 m) and CS19 (1872 m) taken during RV Tangaroa cruise TAN1604. Samples were collected with an Ocean Instruments MC-800 multi-corer (10 cm diameter cores).

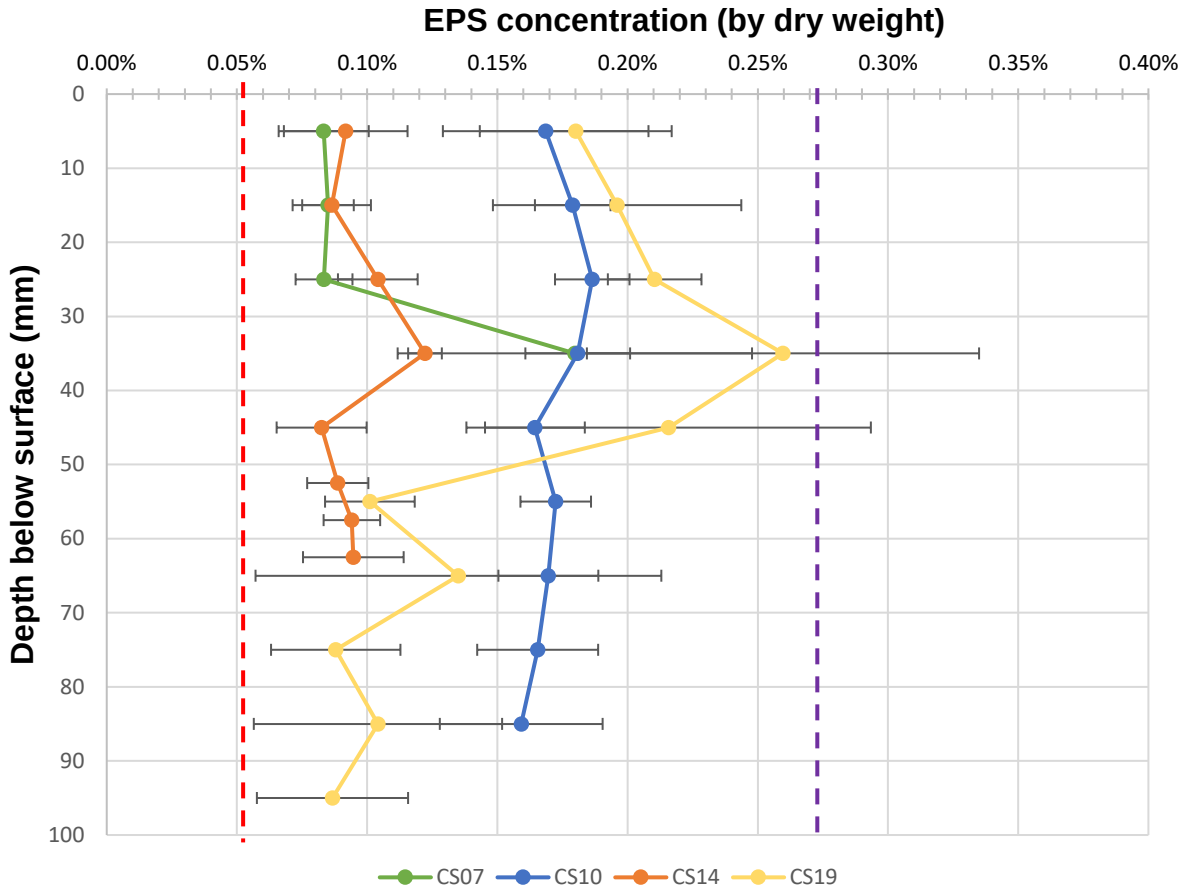

442

443 **Supplementary Figure 3** Vertical profiles of EPS taken from the outer Hauraki Gulf cores
444 offshore New Zealand. The vertical lines represent dry weight quantities of EPS used within
445 the experimental flows: (i) in red, 0.052% EPS in the bed reduced the run-out distance of a
446 23% kaolinite flow from 3.66 m (EPS-free equivalent) to 2.94 m; (ii) in purple, 0.259% EPS
447 in the bed was the maximum amount of EPS used to simulate the 23% kaolinite flows,
448 attaining a reduced run-out distance of 0.6 m. Horizontal lines denote standard deviation of
449 the mean. Error bars correspond to the standard deviations (%) recorded for each EPS
450 concentration (Supplementary Table 1).

451

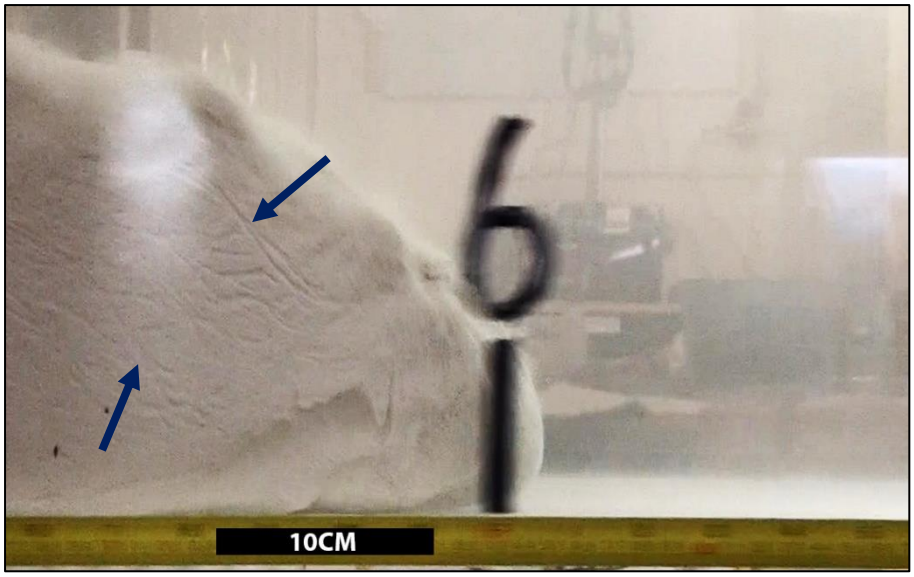

Supplementary Figure 4: Head of F11, 22% clay TTPF without EPS at 1.8 m downstream of flow release. Run-out distance = 4.69 m. Note pronounced coherent fluid entrainment structures indicated by the dark blue arrows. Flow direction is from left to right.

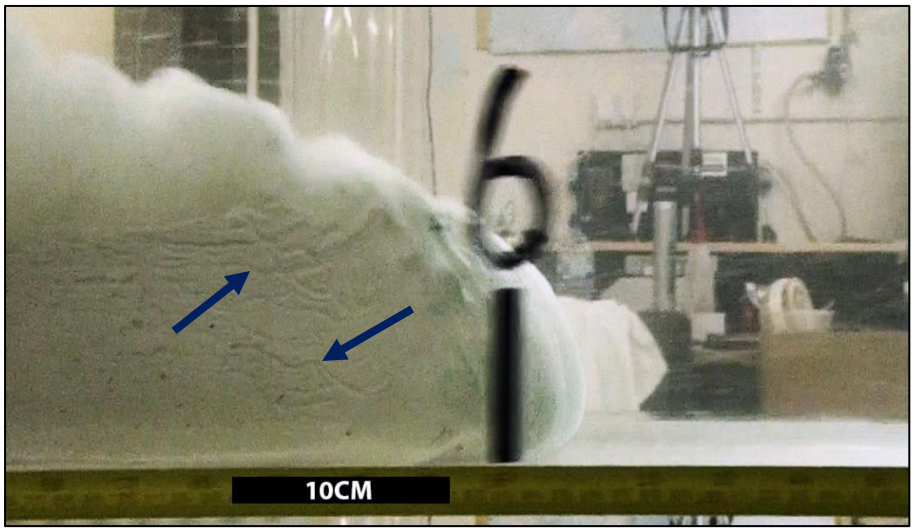

Supplementary Figure 5: Head of F16, 23% clay TTPF without EPS at 1.8 m downstream of flow release. Run-out distance = 3.66 m. Note presence of coherent fluid entrainment structures indicated by the dark blue arrows. Flow direction is from left to right.

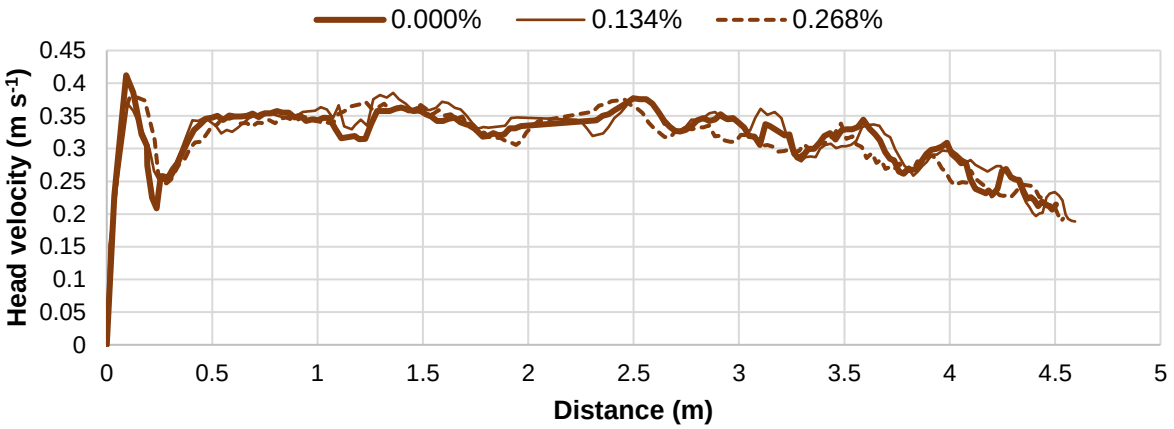

461

462 **Supplementary Figure 6:** Head velocity of 5% kaolinite flows with and without EPS against
463 distance travelled along the tank. Values in legend correspond to EPS concentration added.

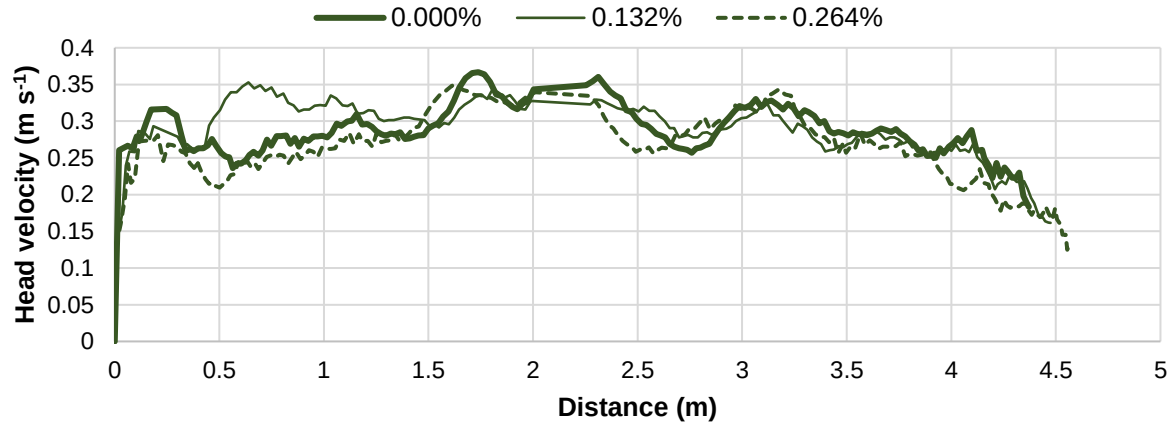

464

465 **Supplementary Figure 7:** Head velocity of 10% kaolinite flows with and without EPS against
466 distance travelled along the tank. Values in legend correspond to EPS concentration added.

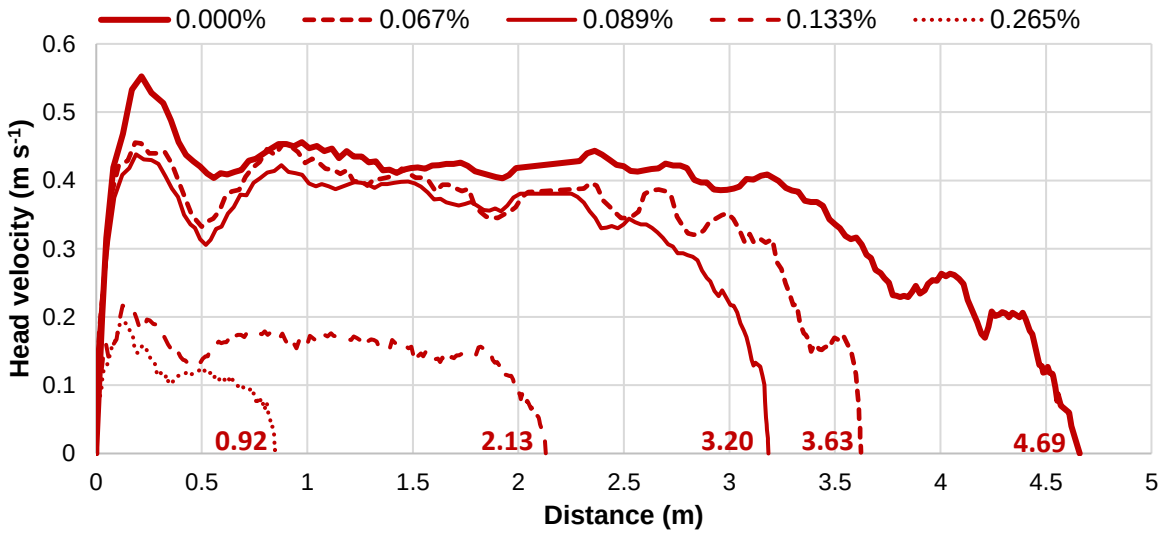

467

468 **Supplementary Figure 8:** Head velocity of 22% kaolinite flows with and without EPS against
469 distance travelled along the tank. Values in legend correspond to EPS concentration added.
470 Numbers above the abscissa indicate run-out distances of flows.

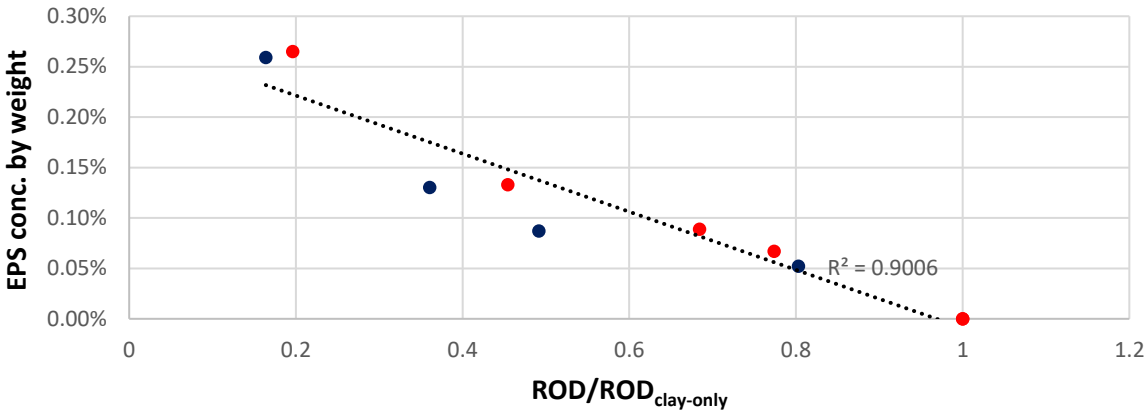

Supplementary Figure 9: Normalized run-out distances of 22% (in red) and 23% (in blue) kaolinite flows with and without EPS against the EPS concentration by weight added to the flow. Run-out distances were normalized to their respective clay-only run-out distance. R^2 = 0.90, p<0.001, n=10.

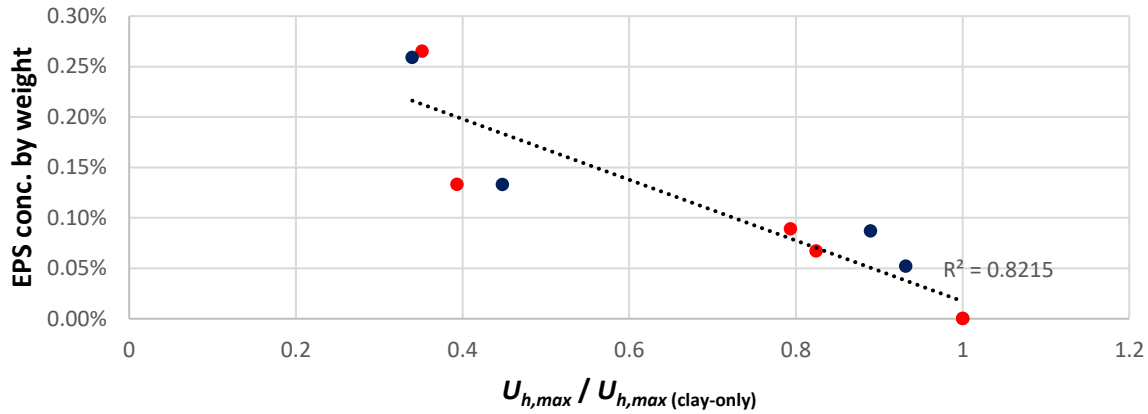

Supplementary Figure 10: Normalized $U_{h,max}$ of 22% (in red) and 23% (in blue) kaolinite flows with and without EPS against the EPS concentration by weight added to the flow. $U_{h,max}$ values were normalized to their respective clay-only $U_{h,max}$ values. R^2 =0.82, p<0.001, n=10.

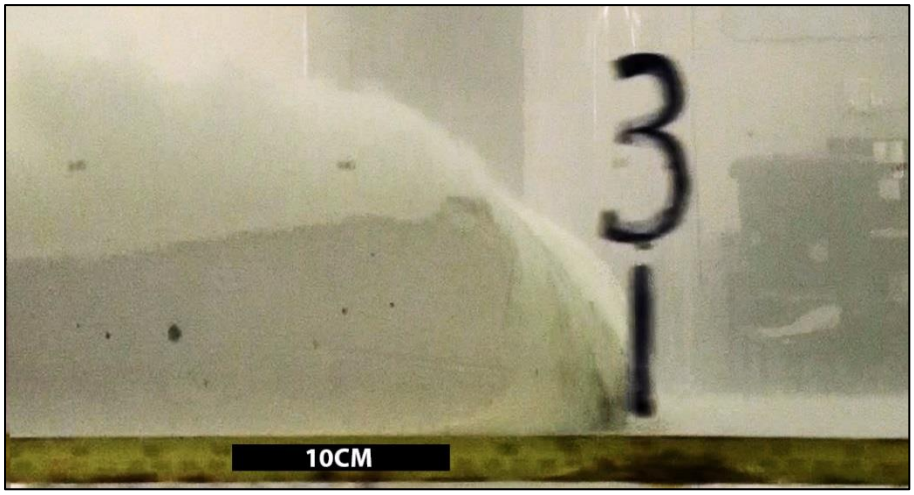

Supplementary Figure 11: Head of F14, 22% clay plug flow with 0.133% EPS at 0.9 m downstream of flow release. Run-out distance = 2.13 m. Note absence of coherent fluid entrainment structures. Flow direction is from left to right.

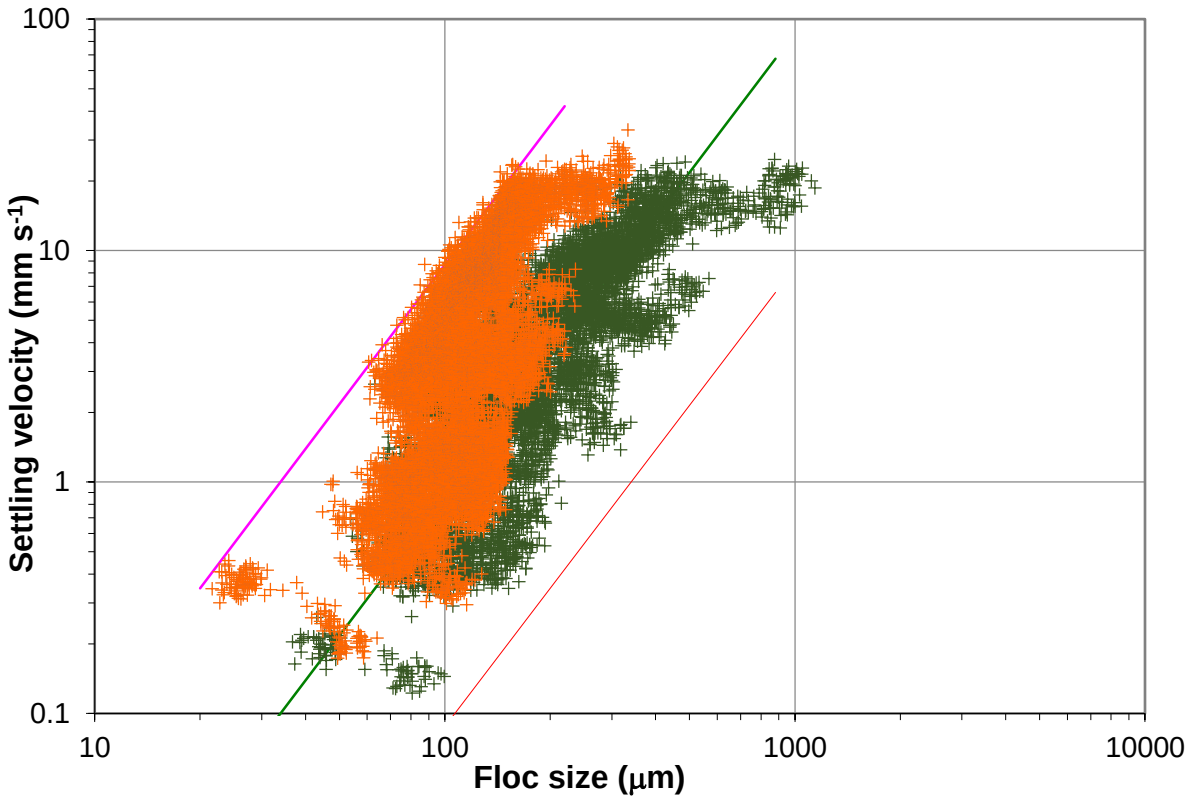

Supplementary Figure 12 Distribution of floc size and settling velocity in samples extracted from the head of the EPS-free 23% kaolinite flow (in orange) and the 23% flow that carried 0.052% EPS (in green). Both samples were collected 12 mm above the base of the tank and at 60% of the respective run-out distance of each flow. Diagonal lines represent contours of constant Stokes-equivalent excess density: 1600 kg m^{-3} (in pink), 160 kg m^{-3} (in green) and 16 kg m^{-3} (in red).